Atrioventricular nodal reentrant tachycardia onset, sustainability, and spontaneous termination in rabbit atrioventricular node model with autonomic nervous system control

Maxim Ryzhii[1,*], Elena Ryzhii[2]

1 University of Aizu, Complex Systems Modeling Laboratory, Aizu-Wakamatsu, Japan
2 Fukushima Medical University, Department of Anatomy and Histology, Fukushima, Japan

* m-ryzhii @ u-aizu. ac. jp

Abstract

Atrioventricular nodal reentrant tachycardia (AVNRT) is one of the most common types of paroxysmal supraventricular tachycardia. The autonomic nervous system (ANS) activity is known to affect sudden episodes of abnormal AVNRT rhythm, but the detailed underlying mechanism is not fully understood. In this work, we update our recent compact multifunctional model of the rabbit atrioventricular node (AV) with ANS control to simulate AVNRT. The refractoriness of model cells is modulated by one ANS coefficient, causing a change in the effective refractory periods, conduction delays, and intrinsic frequency of pacemaker cells. Differences in the effective refractory periods of the slow and fast pathways of the AV node during anterograde and retrograde conduction determine the form of AVNRT. Using the model, we examine the onset, sustainability, and spontaneous termination of typical and atypical forms of AVNRT under ANS modulation. For the first time, the possibility of identifying hidden processes occurring inside the AV node using a computer model is shown, allowing us to come closer to understanding the role of ANS control during AVNRT. The results obtained are consistent with clinical and experimental data and represent a new step toward understanding the electrophysiological mechanisms of this type of arrhythmia.

Introduction

The atrioventricular (AV) node consists of dual pathways: a fast pathway (FP) with a relatively longer effective refractory period (ERP) and a slow pathway (SP) with a shorter ERP. These pathways can create a reentrant circuit, a substrate for AV nodal reentrant tachycardia (AVNRT), the most common type among the regular supraventricular arrhythmias [1].

AVNRT manifests as sudden episodes of a few cycles of abnormally fast heartbeats (reciprocal or echo beats) or as sustained or persistent tachycardia. AVNRT is electrophysiologically classified as typical (slow-fast) and atypical (fast-slow, and also slow-slow in humans) forms corresponding to anterograde-retrograde conduction sequence through the dual AV nodal pathways [2].

The autonomic nervous system (ANS) plays an essential role in initiating and terminating supraventricular tachycardias in the AV node [3]. Sympathetic stimulation

usually facilitates the induction of AVNRT, whereas enhancement of vagal tone through pharmacological administration or Valsalva maneuvers is commonly used to terminate the tachycardia [4, 5]. The effect of ANS control on dual pathways interaction in the initiation, sustainability, and spontaneous termination of AVNRT is still not well understood despite some attempts to explain its exact underlying physiological mechanism.

A few functional computer models of AV node were developed [6–8], but to our knowledge only one of them incorporates ANS control [8]. In the latter model, the authors modulate vagal tone by modifying parameters of AV node refractoriness and conduction velocity separately. Recently, we have developed a compact, multi-functional rabbit AV node model based on the simplified two-variable cardiac cell model [9]. The one-dimensional model includes dual pathways, primary pacemaking in the sinoatrial node (SN), and subsidiary pacemaking in SP and is tuned to the available experimental data. Visualization of interactions between intact and post-ablated SP and FP in the form of Lewis ladder diagrams facilitates the study of AVNRT.

Experimental observations show that FP has a significantly longer effective refractory period (ERP) in the case of anterograde conduction (aERP_{FP}) than that of SP (aERP_{SP}), which is a substrate for typical slow-fast AVNRT at stimulation periods shorter than the aERP_{FP} [10]. This substantial property of normal AV node behavior, demonstrated by simulation and experimental studies [6, 7, 11], provides effective conduction slowing and fast rhythm filtering. In contrast, in the case of retrograde conduction with His bundle pacing no apparent difference between retrograde ERPs of SP (rERP_{SP}) and FP (rERP_{FP}) was observed in both control and post-ablation cases. Taking into account the statistical uncertainty of the difference between rERP_{SP} and rERP_{FP} [10], in our preliminary work [12], we assumed that any relationship between rERP_{SP} and rERP_{FP} values may exist within a reasonable range. We showed that rERP_{SP} and rERP_{FP} affected insignificantly the anterograde conduction in the AV node. Along with the typical AVNRT of atrial origin, we simulated both typical and atypical AVNRT forms with His bundle pacing and demonstrated that the difference in aERP and rERP of FP and SP determines the form of AVNRT. However, these results did not take into consideration the influence of ANS control.

To overcome this drawback, we updated the functionality of our AV node model incorporating the ANS control. The sympathetic and vagal (parasympathetic) control was implemented by including only one coefficient for scaling parameters related to the refractoriness of model cells. Other main cardiac conduction system properties, such as intrinsic rates of pacemakers and conduction times, depend on this coefficient.

In the current work, using the modified model, we study the onset, susceptibility, and spontaneous termination of typical and atypical forms of AVNRT. We consider the induction of AVNRT not only by premature atrial and His bundle stimulation, referred to in clinical practice as premature atrial (PAC) and ventricular (PVC) complexes, but also by electrical impulses originating within AN node (premature junctional complex, PJC) [1].

Model and Methods

The scheme of the compact AV node model used in this study is shown in Fig. 1. Each model cell is described by Aliev-Panfilov cardiac cell model [13] given by a couple of reaction-diffusion type ordinary differential equations

$$\dot{V} = c[kV(V - a_1)(1 - V) - rV] + I^{coupl} + I^{stim}, \tag{1}$$

$$\dot{r} = c\epsilon[-r - kV(V - a_2 - 1)], \qquad \epsilon = \epsilon_0 + r\mu_1/(V + \mu_2), \tag{2}$$

where V is the dimensionless transmembrane potential, r is the gate variable, c is the time scaling coefficient, and k is the parameter controlling the magnitude of the

transmembrane current. Parameters ϵ_0, a_1, a_2, μ_1, and μ_2 determine the conduction characteristics of tissue, $a_1 > 0$ represent the excitation threshold of quiescent excitable cells, while $a_1 < 0$ sets the intrinsic oscillation frequency of the pacemaking cells (gray-shaded in Fig. 1) [14].

The intercellular coupling terms

$$I_i^{coupl} = d_{i-1}(V_{i-1} - \beta_{i-1}V_i) + d_i(-V_i + \beta_i V_{i+1}) \tag{3}$$

in the one-dimensional system account for the coupling asymmetry, where d_i are the diffusion coefficients (normalized on dimensionless distance), i denotes the index of neighboring cells, and the coefficients $\beta < 1$ correspond to the accelerated anterograde and slowed retrograde conduction, and vice versa for $\beta > 1$. I^{stim} denotes external stimulation current applied to the atria or His bundle (thick arrows in Fig. 1) to perform S1S2 and S1S1 stimulation protocols.

The standard S1S2 stimulation consisted of nine pulses with constant basic S1–S1 interval equal to spontaneous sinus rhythm interval determined by the current ANS state, and S2 test premature stimulus with S1–S2 interval introduced with a decrement of 1 ms until conduction through AV node is blocked. The S1S2 conduction time was measured between AM2 and HB1 model cells.

The S1S1 stimulation was performed by applying ten pulses with 1 ms interval decrement starting from spontaneous sinus rhythm interval at the current ANS state. For this stimulation type, we measured atria-His and His-atria conduction delays within the AV node ring between AM3 and PB model cells. Both atrial and His bundle stimulation pulses were 1 ms long and 1.3 times above the threshold.

We implemented the effect of the ANS in our rabbit cardiac conduction system model by the introduction of a control coefficient γ, allowing dynamical changing of the parameters μ_1 and μ_2 responsible for the cell refractoriness [13]:

$$\mu_1^* = \mu_1/\gamma, \qquad \mu_2^* = \mu_2\gamma, \qquad \epsilon = \epsilon_0 + r\mu_1^*/(V + \mu_2^*). \tag{4}$$

To reflect the different states of the ANS, the same coefficient γ was simultaneously applied in all model cells of the part of the cardiac conduction system (Fig. 1) from the sinus node (SN) to the penetrating bundle (PB), including AV junctional pacemaker [15].

Since only isolated rabbit heart preparations were used in the experiments [7,10,11], any influence of the ANS was absent, leaving the hearts in a state representing a static invariable situation regarding the cardiac conduction system. At such conditions, the onset of AVNRT was observed in the S1S2 protocol stimulation at short atrial test pulses with a normal sinus rhythm of about 166 bpm (360 ms beating interval) [10]. However, it is known that enhancing sympathetic tone may provoke AVNRT onset [16]. At the same time, Valsalva maneuver or adenosine administration [4, 5] causes the vagal tone enhancement, resulting in reduced heart rate and consequent termination of AVNRT. Considering the above facts, we set $\gamma = 1.0$ corresponding to an augmented sympathetic tone state with high sinus rhythm, allowing induction of some form of AVNRT. An increase of γ first leads to a normal rhythm at $\gamma \simeq 1.7$ and then to bradycardia when the vagal tone dominates ($\gamma \simeq 2.0$). A decrease of γ means enhancement of sympathetic tone and, respectively, shortens the refractory period, action potential duration of the affected model cells, and ERP of both pathways, reduces nodal conduction time, and increases intrinsic rates of the sinus node and AV nodal pacemakers [17].

The three AV node model variants considered had similar anterograde conduction characteristics (aERP_{SP} ¡ aERP_{FP}) but different retrograde conduction properties [12]. We kept $\mathrm{rERP}_{SP} \simeq \mathrm{rERP}_{FP}$ for increased sinus rhythms (sympathetic tone) in the *first model variant*. The *second model variant* had slightly reduced diffusion coefficient d for the last three FP cells and increased d for the last four SP cells compared with the

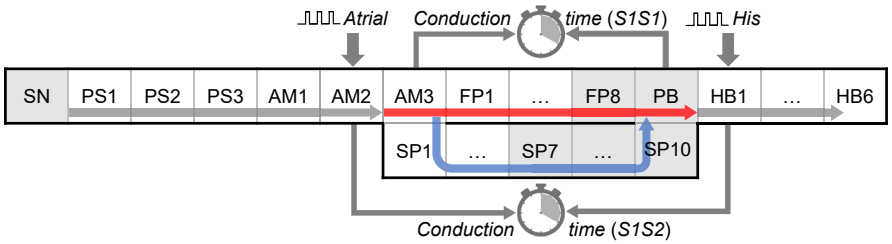

Fig 1. Schematic representation of the rabbit atrioventricular node model. SN - sinus node, PS - peripheral sinus node cells, AM - atrial muscle cells, FP - fast pathway cells, SP - slow pathway cells, PB - penetrating bundle cell, HB - His bundle cells. Thick vertical arrows denote places of stimuli application for atrial and His bundle pacing. The arrows within the structure correspond to normal conduction. The gray shading indicates pacemaker cells.

first variant to provide longer rERP_{FP} within the whole range of γ. The *third model variant* had the coupling asymmetry coefficient β reduced five times between SP10 and PB model cells, creating the relationship rERP_{SP} ¿ rERP_{FP} at higher rhythms (sympathetic tone) and its inversion (rERP_{SP} ¡ rERP_{FP}) at normal and reduced rhythms (vagal tone). The refractory period in the proximal part of His bundle (HB1–HB3 cells) was reduced in the second and third model variants compared to the first to facilitate His bundle premature stimulation.

For each model variant, we considered three scenarios of premature cardiac complexes classified by their origin - atrial (PAC), ventricular or His bundle (PVC), and AV intranodal or junctional (PJC). The cases of PAC and PVC required proper selection of premature extrastimulus interval within the AVNRT induction window. In PJC, a short burst of sympathetic activity with high sinus tachycardia was applied to stimulate the conduction block within the AV node.

The ANS coefficient γ was dynamically varied step-wise during the simulations at predefined moments. The intervals between changing γ were selected to reflect the natural reaction of cardiac conduction to ANS modulation.

The simulations were conducted with MATLAB R2023a, using its *ode23* function to solve the ordinary differential equations. Other parameter values were similar to that in [9] and are based on rabbit experimental data [10,11]. Additional details of the basic rabbit AV node model and its properties can be also found in [9].

Results

In what follows, we refer to AVNRT as sustained oscillations within the AV ring and echo beats (reciprocating pulses) as decaying oscillations with a few cycles.

The first model variant

Figure 2 demonstrates simulation results of AVNRT onset and spontaneous termination for the first model variant under ANS control. The top panels demonstrate ladder diagrams of conduction propagation from the sinus node to His bundle via FP (red) and SP (blue color). The value of the current ANS coefficient γ and corresponding sinus rate (in brackets) are indicated above the ladder diagrams. Vertical dashed lines indicate the coefficient switching moments. The middle and bottom panels show action potential sequences from the sinus node to His bundle separately for FP and SP.

In Fig. 2(a), we started with a slightly increased sinus rate at $\gamma = 1.5$ with the application of premature atrial stimulus (indicated by black arrowhead), causing a couple of slow-fast echo beats followed by sinus rhythm. Applying PAC at γ decreased to 0.8,

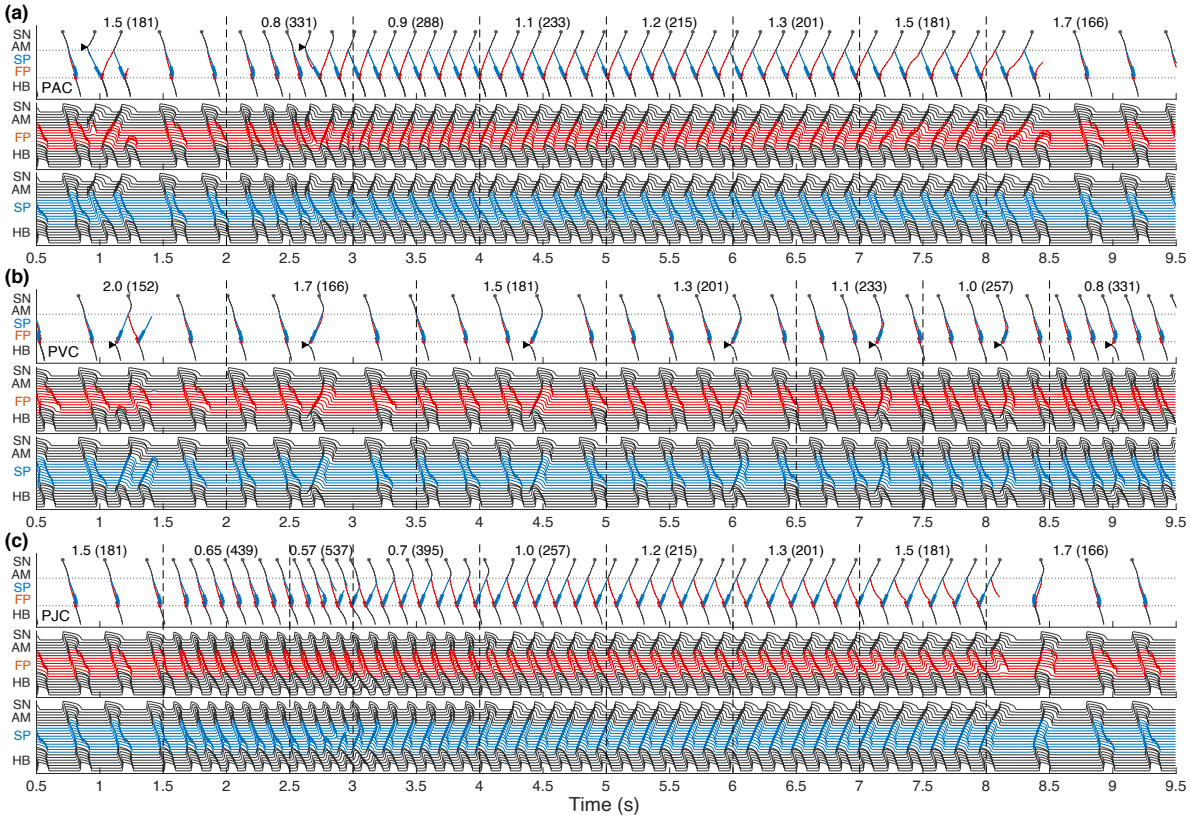

Fig 2. The first model variant with $\mathrm{rERP}_{SP} \simeq \mathrm{rERP}_{FP}$. The top panels show the ladder diagram of the excitation propagation in the AV nodal dual pathway structure from SN to HB through FP (red traces) and SP (blue traces). The numbers above the diagrams indicate the value of the coefficient γ and corresponding sinus rhythm in bpm (in brackets). Larger circle marks correspond to the pacemaker cells. Black arrowheads denote place and moments of premature stimulation. Middle and bottom panels demonstrate action potentials passing via FP and SP. (a) Onset of typical AVNRT with atrial premature stimulation (PAC) at enhanced sympathetic tone followed by spontaneous termination at rising vagal tone. (b) No AVNRT induction was observed with His bundle stimulation (PVC) within practically the whole range of the ANS coefficient. (c) A short burst of high sinus rhythm (PJC) caused atypical AVNRT.

we obtained the onset of typical AVNRT. The oscillations persisted with increasing γ up to 1.5 and simultaneous decreasing of heart rate and spontaneously terminated at $\gamma = 1.7$ with a return to the normal sinus rhythm.

With His bundle premature stimulation (PVC), trying to provoke AVNRT at different γ, we obtained only an echo beat during bradycardia with $\gamma = 2.0$ [Fig. 2(b)].

AVNRT with PJC originates from within the AV node, so it may not require an external premature stimulus. A short episode with a sudden decrease of γ to the very low value of 0.57 with a very high sinus rhythm of 537 bpm led to a critical reduction of action potential duration and amplitude and block of SP conduction. This triggered atypical AVNRT, which persisted with increasing γ until the latter reached a normal value of 1.7 [Fig. 2(c)].

To investigate the underlying physiological background of the results in Fig. 2, we performed simulations with S1S2 and S1S1 stimulation protocols. Figure 3 presents various related conduction curves for the first model variant calculated for different ANS states represented by the coefficient $\gamma = 0.8$, 1.0, 1.2, 1.5, and 1.7.

Figures 3(a) and 3(b) demonstrate anterograde and retrograde conduction curves

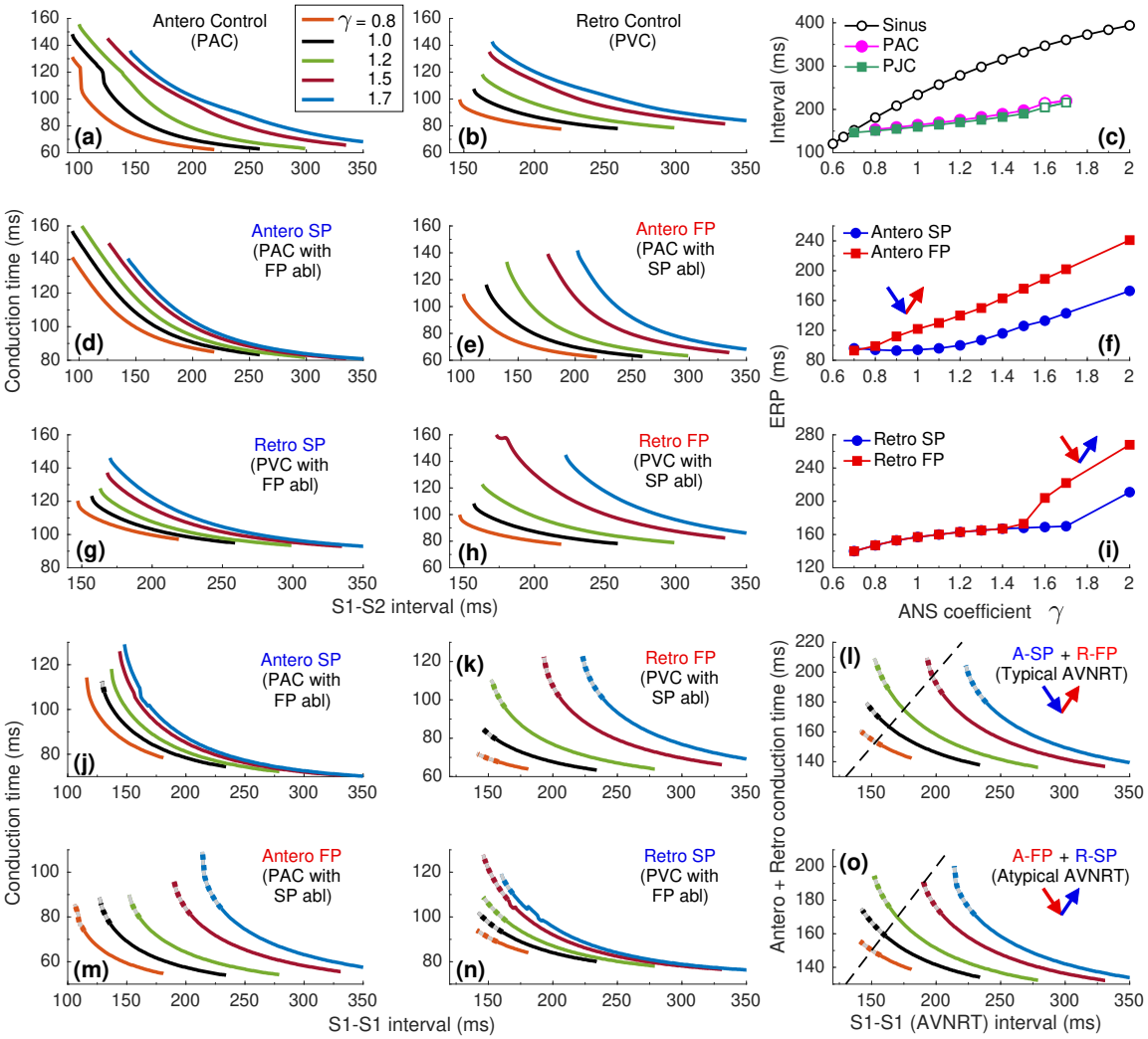

Fig 3. Conduction characteristics for S1S2 (a)–(i) and S1S1 (j)–(o) stimulation protocols for the first model variant. (a) Control case with atrial stimulation (PAC); (b) control case with His bundle stimulation (PVC); (c) dependence of sinus rhythm and AVNRT intervals of atrial (PAC) and AV intranodal (PJC) origin on the coefficient γ; (d) and (e) - anterograde conduction times for SP and FP, and their ERPs (f); (g) and (h) - retrograde conduction times for SP and FP, and their ERPs (i); (j) and (k) - anterograde SP and retrograde FP conduction times and their sum versus typical AVNRT interval (l); (m) and (n) - anterograde FP and retrograde SP conduction times and their sum versus atypical AVNRT interval (o). Unstable conduction is indicated by thick dotted lines. Black dashed lines are the AVNRT sustainability lines.

for the control (intact) AV node. With decreasing γ, i.e., increasing sympathetic tone, the anterograde conduction switching from FP to SP became more pronounced with sharper tilt [Fig. 3(a)].

The right ends of the curves are limited by spontaneous sinus rhythm interval, which decreases with smaller γ [Fig. 3(c)]. Apart from the sinus rhythm interval, ANVRT intervals obtained with PAC and PJC shown in Figs. 2(a) and 2(c) are indicated in Fig. 3(c) by filled markers, and echo beats (at $\gamma = 1.6$ and 1.7) - by open markers. The intervals of AVNRT of different origins are always shorter than the sinus rhythm interval and indicate the overdrive suppression of the latter by the reentrant oscillations.

The S1S2 conduction curves obtained for individual SP and FP pathways (post-

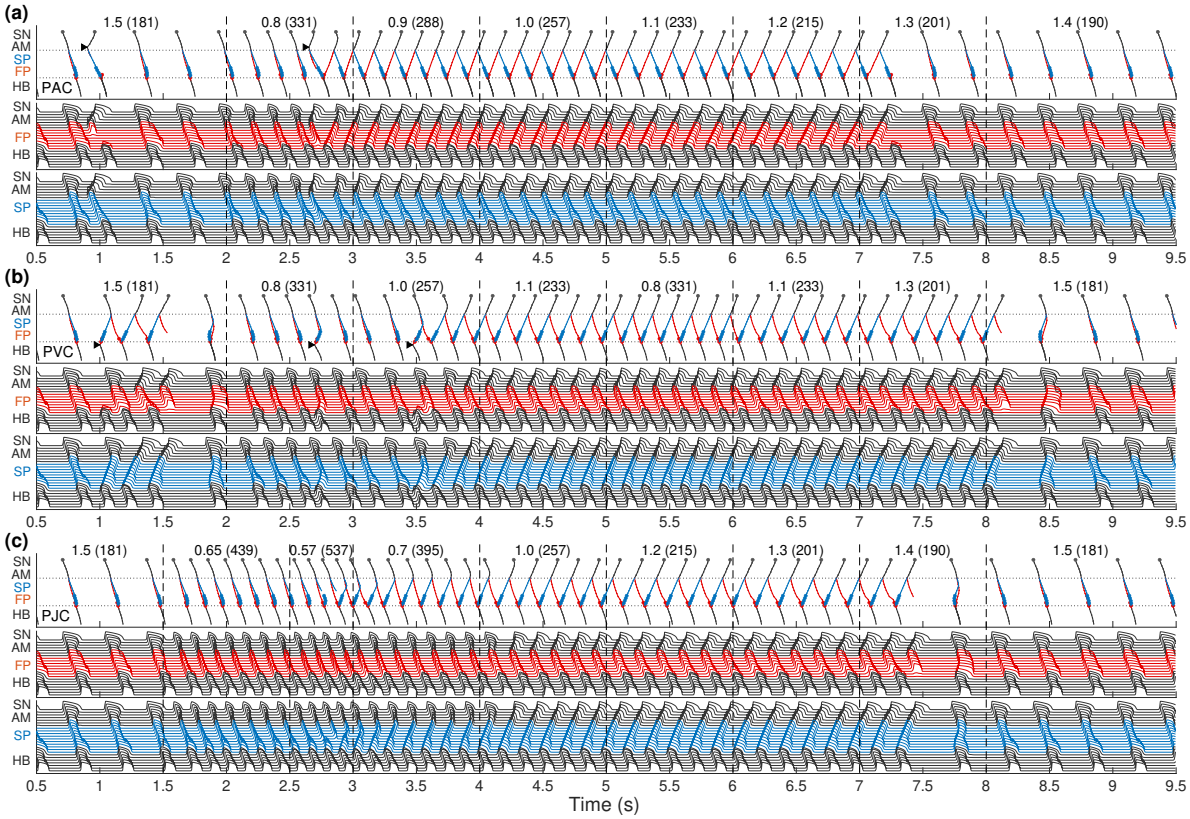

Fig 4. The same as in Fig. 2 but for the second model variant with $\mathrm{rERP}_{SP} < \mathrm{rERP}_{FP}$.

ablation cases) and the dependence of their ERPs on γ for PAC and PVC are shown in Figs. 3(d)–3(f) and 3(g)–3(i), respectively. The distance between FP-only curves with changing γ is more pronounced for both atrial and His bundle stimulation. Within the whole useful range of γ, aERP_{SP} is smaller than aERP_{FP} [Fig. 3(f)]. This is common for mammalian AV node [10] and creates a possibility of typical AVNRT onset within the wide range of ANS states. On the other hand, the retrograde ERPs of both pathways (rERP_{SP} and rERP_{FP}) are equal within the whole range of sympathetic tone [Fig. 3(i)]. The above relationships between the SP and FP ERPs allowed the onset of typical AVNRT with atrial pacing at $\gamma \geq 0.8$ [Fig. 2(a)], and blocked the initiation of atypical AVNRT with His bundle pacing at $\gamma \leq 1.5$ [Fig. 2(b)].

AVNRT is a self-sustained oscillation with a cycle length equal to the stimulation period. Thus, in the AV ring with initiated reentrant excitation, its period should be equal to the sum of anterograde SP and retrograde FP conduction times for the typical AVNRT form and anterograde FP and retrograde SP conduction times for the atypical form. The sustainability of periodic oscillations in the AV ring can be checked by a crossing point between the sum of the pathway conduction times and the identity (y = x) or the sustainability line of the AVNRT cycle.

Figures 3(j)–3(l) show the conduction time calculated with S1S1 protocol for anterograde SP, retrograde FP and their sum for typical AVNRT form, and Figs. 3(m)–3(o) - anterograde FP and retrograde SP and their sum for atypical form. The thin black dashed lines denote the AVNRT sustainability lines.

In our simulations, the initial time delay before applying the first stimulus of the S1S1 protocol affected the stability of conduction in pathways and, consequently, the

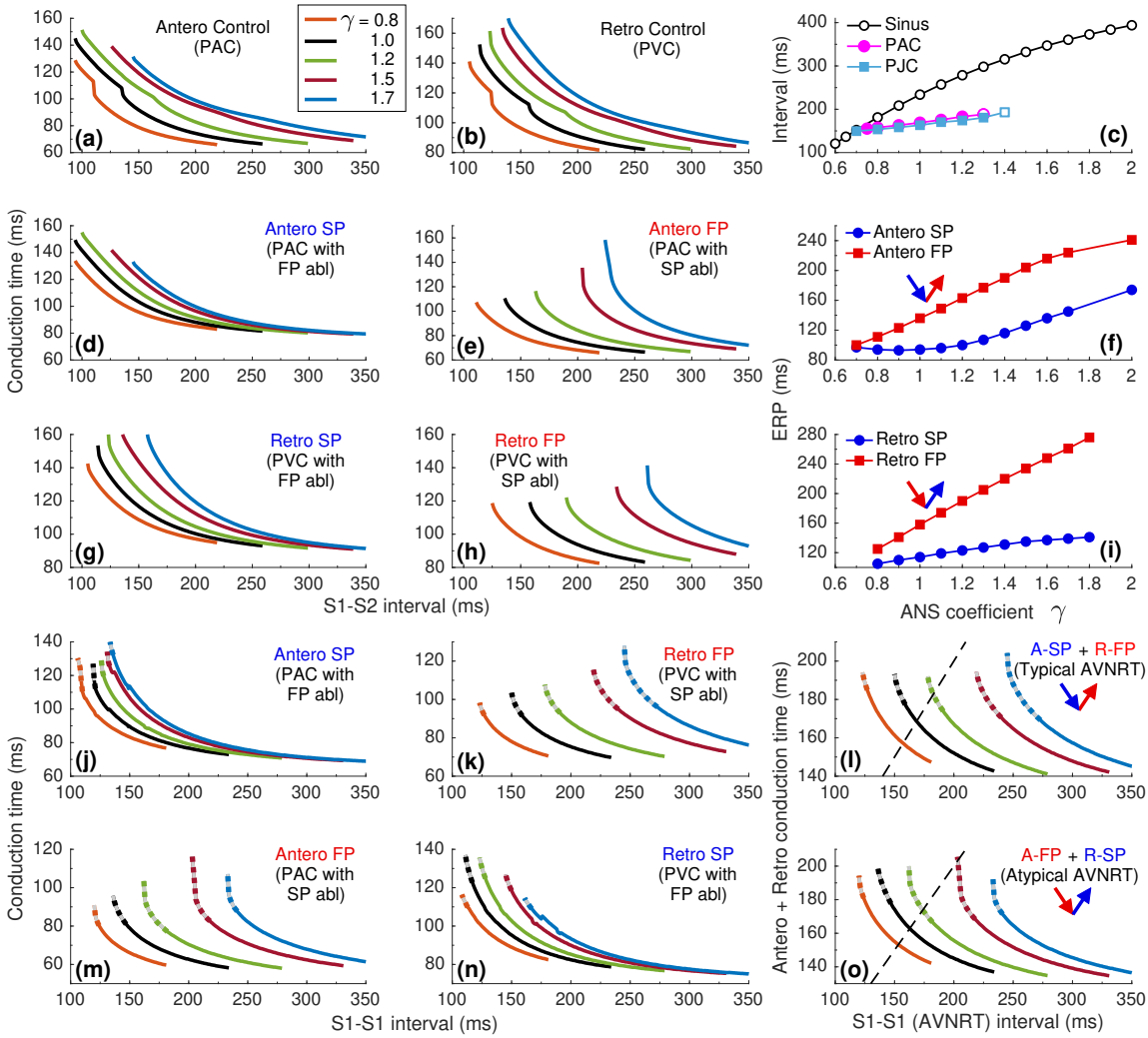

Fig 5. The same as in Fig. 3 but for the second model variant.

sustainability of AVNRT. The variation of the initial delay resulted in the unstable behavior of the conduction curves at short S1S1 intervals [left ends of the conduction curves in Figs. 3(j), 3(k), 3(m), and 3(n)]. The unstable regions are marked by thick dotted lines on both individual pathway conduction and their summation curves in Figs. 3(l) and 3(o). Note, that the earliest point on each summation curve and the width of its unstable region are determined by whichever pathway curve has a higher ERP. In addition, some cases of conduction alternans [18] in the pathways were observed, which are reflected in a few bumps on the curves [Figs. 3(j) and 3(n) and figures below].

It is seen from Fig. 3(l) that a persistent form of typical AVNRT indeed exists for $\gamma = 1.0$ and 1.2 (intersection of AVNRT sustainability line with solid conduction lines), can exist depending on initial conditions for $\gamma = 0.8$ and 1.5 (intersection with dotted conduction lines), and does not exist for $\gamma = 1.7$ (no intersection of AVNRT sustainability line with conduction lines). This explains slow-fast echo beats at $\gamma = 1.5$, sustained oscillations at the same γ later upon switching from 1.3, and spontaneous AVNRT termination at $\gamma = 1.7$ [Fig. 2(a)]. The behavior of the cycle curves in Fig. 3(o) basically coincides with that in Fig. 3(l), with similar stability conditions for atypical

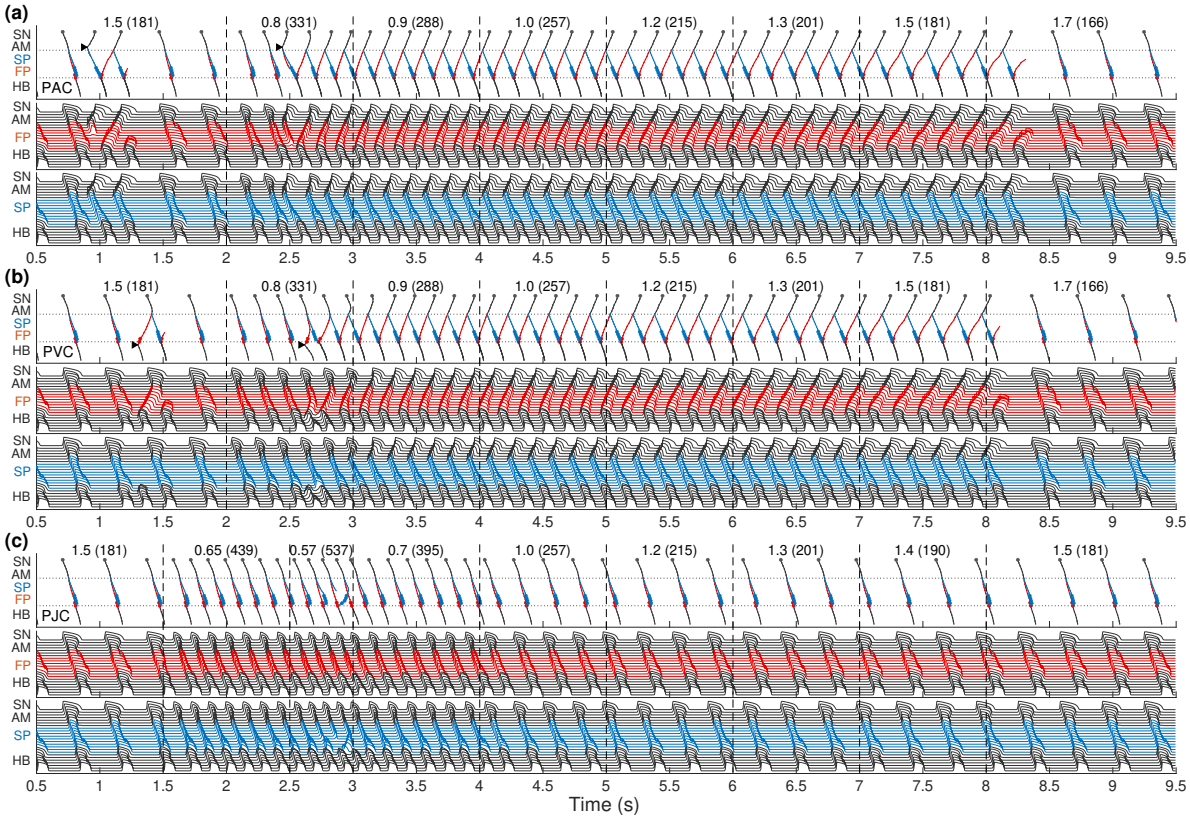

Fig 6. The same as in Fig. 2 but for the third model variant with a significant decrease of coupling asymmetry in the posterior node extension of SP, reducing its coupling in the retrograde direction ($\mathrm{rERP}_{SP} > \mathrm{rERP}_{FP}$) and slowing the retrograde SP conduction.

AVNRT, which most likely can only have an intranodal AV origin [type PJC, Fig. 2(c)]. According to Fig. 3(i), atypical AVNRT can be initiated by His bundle pacing at $\gamma \gtrsim 1.5$, but in this range of γ the sustainability condition in Fig. 3(o) is not fulfilled, resulting in only a single fast-slow echo beat at $\gamma = 2.0$ [Fig. 2(b)]. As marked by dotted lines in Fig. 3(o), for $\gamma \simeq 0.8$ and 1.5 the sustainability of atypical AVNRT forms also depends on the preceding conditions.

The second model variant

Figures 4 and 5 present results with a similar simulation setup but for the second model variant with $\mathrm{rERP}_{SP} < \mathrm{rERP}_{FP}$.

In Fig. 4(a) for atrial stimulation, we observed a similar situation as in Fig. 2(a), but spontaneous termination of typical AVNRT took place earlier at smaller $\gamma = 1.3$. His bundle stimulation yielded different results [Fig. 4(b)]. First, a few fast-slow echo beats appeared with $\gamma = 1.5$. Further, starting to increase γ from low values, we were able to induce atypical AVNRT only at $\gamma \geq 1.0$. Sustained oscillations in the AV ring continued until γ reached 1.5. Like the first model variant, the model states at $\gamma \simeq 0.8$ and 1.5 seem unstable and depend on the preceding conditions.

It was also possible to induce the PJC type of atypical AVNRT with a sudden decrease of γ to 0.57 in the same manner as for the first model variant. In this case, AVNRT persisted with increasing γ up to 1.4 [Fig. 4(c)].

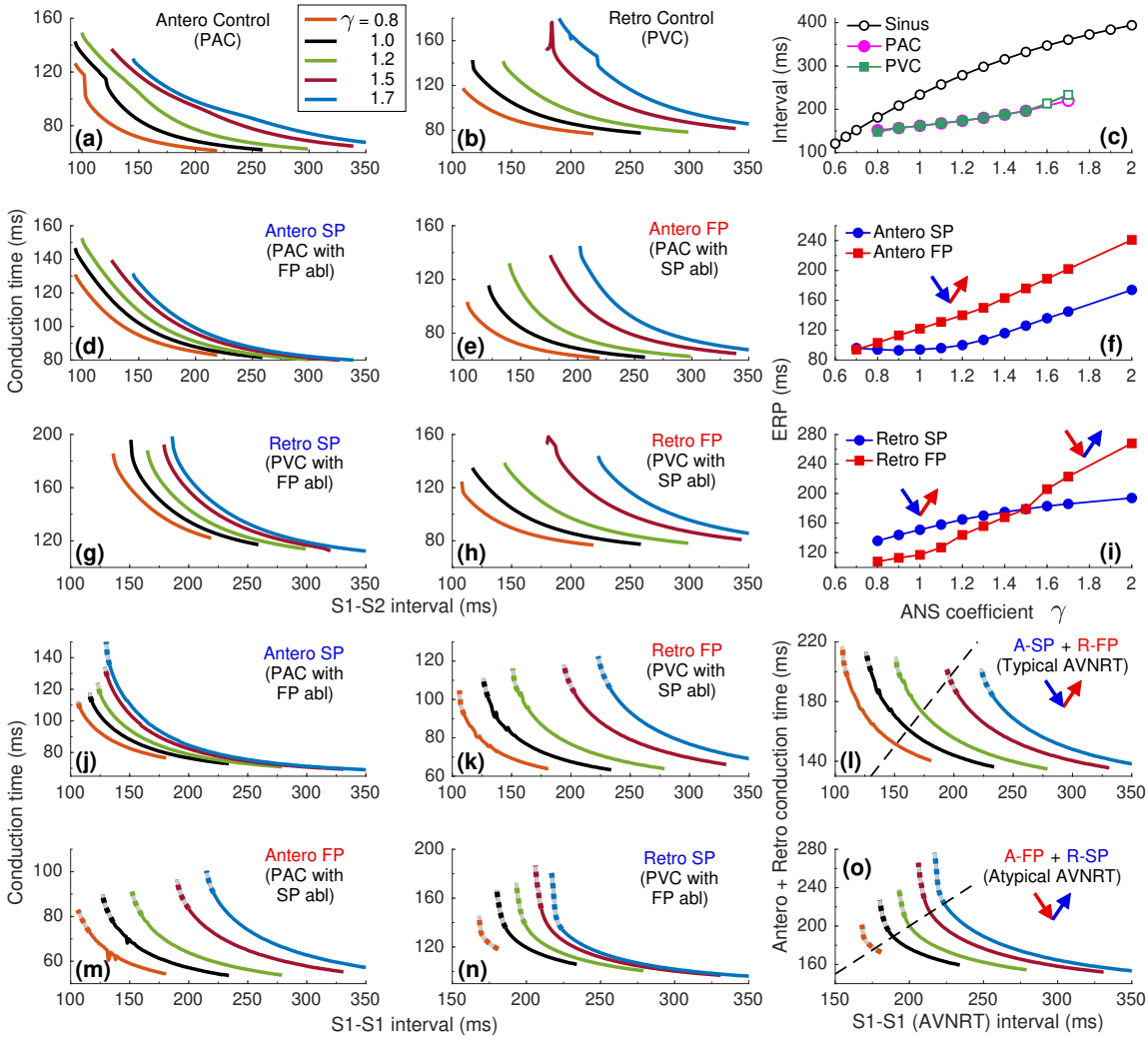

Fig 7. The same as in Fig. 3 but for the third model variant where the retrograde conduction was slowed in SP, leading to significantly increased rERP_{SP} (g). The anterograde SP conduction is virtually similar to the first model variant (d).

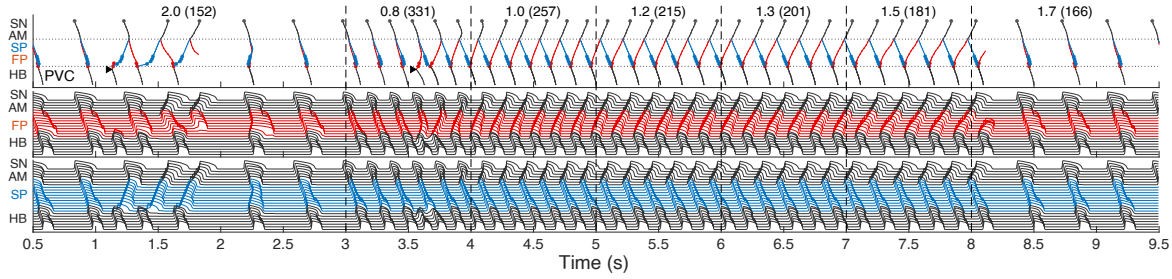

Fig 8. Premature His bundle pacing in the third model variant at $\gamma = 2.0$ induced a few fast-slow echo beats.

The anterograde S1S2 conduction curves [Figs. 5(a), 5(d), and 5(e)] and the relationship of anterograde ERPs between SP and FP [Fig. 5(f)] remained similar to those of the first model variant [Fig. 3(f)]. However, the tilt related to the conduction switching from FP to SP appeared on the retrograde control curves [Fig. 5(b)]. It

became sharper with decreasing γ, due to the increase of rERP_{FP} introduced in this model variant and reflected in Figs. 5(h) and 5(i) with relatively wide induction window for atypical AVNRT. A wider induction window corresponds to higher inducibility of AVNRT or echo beats [19].

As seen from Figs. 4(a) and 5(l), the sustainability of typical AVNRT persisted only at $\gamma < 1.3$. Interestingly, with His bundel pacing at $\gamma = 0.8$, neither AVNRT nor echo rhythms were induced [Fig. 4(b)], while atypical AVNRT initiated at higher values of γ persisted at the same value $\gamma = 0.8$. For atypical AVNRT upper limit was $\gamma < 1.4$ [Figs. 4(c) and 5(o)].

The third model variant

Simulation results obtained with the third model variant are demonstrated in Figs. 6 and 7. The situation with typical AVNRT induction [Fig. 6(a)] looks like that in Figs. 2(a) and 4(a) due to the similarity of anterograde conduction and refractory curves in panels (d)–(f) of Figs. 3, 5, and 7. However, with the PVC we obtained the same typical form of AVNRT as for PAC [Fig. 6(b)]. At $\gamma = 1.5$, both slow-fast echo beat and typical AVNRT were initiated depending on preceding conditions. This situation is supported by the retrograde ERP curves in Fig. 7(i) and typical AVNRT sustainability curves in Fig. 7(l). In Fig. 7(i), the retrograde ERP curves are crossing at $\gamma = 1.5$, which suggests induction of typical AVNRT in the $\gamma < 1.5$ range, and possible induction of atypical AVNRT at $\gamma > 1.5$. The peculiarity of the point $\gamma = 1.5$ is reflected in the unusual form of retrograde control and FP conduction curves near the ERP point in Figs. 7(b) and 7(h).

As seen from Fig. 6(c), in contrast to the first and second model variants, for the third model variant neither AVNRT nor echo beats were initiated from within the AV nodal ring with a sudden decrease of γ.

While the sustainability curves in Fig. 7(o) suggest the possibility of sustained atypical AVNRT at $\gamma > 0.8$, we were unable to provoke the atypical form of the tachycardia at γ values slightly above the perculatity point [Fig. 6(b)]. Nevertheless, we managed to induce some fast-slow echo beats at bradycardia with $\gamma = 2.0$ (see Fig. 8).

Discussion

Using our compact multifunctional model of rabbit AV node, we simulated the effect of ANS on the behavior of AVNRT. Incorporating a single ANS coefficient γ allowed the introduction of the combined effect of sympathetic and parasympathetic activity into the basic AV node model through the modulation of the refractoriness of model cells. A decrease in γ increases sympathetic tone, diminishes parasympathetic tone, and leads to a reduction in AV nodal conduction time and nodal refractory period in accordance with the results of electrophysiological studies [20, 21]. On the other hand, parasympathetic activity dominates with increasing γ and has opposite effects on AV nodal conduction time and refractory period [22]. The approach is somewhat similar to one used in the work [8]. Still, our model utilizes a one-dimensional reduced-order reaction-diffusion system composed of 32 model cells and one ANS control coefficient.

The validity of our approach on incorporation of ANS control into our rabbit AV node model and obtained results are supported by the following clinical and experimental observations.

Clinical studies suggest that sustained typical AVNRT episodes are preceded by an increase in sympathetic tone [3]. Accordingly, for the induction of AVNRT in most

cases, we set γ to a small value (0.80–1.0) and obtained slow-fast AVNRT [Figs. 2(a), 4(a), and 6(a)].

The atypical AVNRT form appeared in our simulation in rare cases with PJC, which occur primarily in children and postoperative patients [23] [Figs. 2(c) and 4(c)], in the case with PVC with rERP_{SP} ¡ rERP_{FP} [24] [Fig. 4(b)], and in even more marginal case with PVC at high vagal tone [Figs. 2(b) and 8]. These results are supported by the clinical fact of the much more frequent appearance of the typical form of AVNRT than the atypical one [25].

As described in [26], under certain conditions, the difference in retrograde ERPs between SP and FP may become inverted with the changing of the ANS state [Fig. 7(i)], resulting in both typical and atypical AVNRT forms can present in the same subject. In Fig. 8, the fast-slow echo beats were induced with enhanced vagal tone ($\gamma = 2.0$) and slow-fast AVNRT appeared in $0.8 \leq \gamma \leq 1.5$ range. In some patients, the onset of AVURT occurred throughout periods of increased vagal tone, such as during sleep [17], which is consistent with our result shown in Fig. 8.

While the onset of AVNRT is mostly observed at enhanced sympathetic activity, a possibility exists for the tachycardia or reciprocating beats induction with increased vagal tone due to the widening of the induction window [17, 19]. With increasing parameter γ and decreasing sinus rate, the inducibility of typical AVNRT by atrial extrastimulus strengthened in all model variants [Figs. 3(f), 5(f), and 7(f)]. We also observed the same effect of ANS on the atypical AVNRT inducibility by His bundle stimulation for the second model variant [Fig. 5(i)].

The *initiation* of AVNRT requires three factors: (a) a specific ANS state providing proper refractoriness and conduction time of the AV nodal pathways, (b) a difference in ERPs between the slow and fast pathways, and (c) premature atrial or ventricular stimulus with proper timing. The latter condition is unnecessary when AVNRT originated within the AV node (PJC). Induction of AVNRT by short bursts of fast sinus rhythm or atrial pacing was reported in patients [17]. Similar phenomena is seen in Figs. 2(c) and 4(c).

The *sustainability* of AVNRT is determined by the coincidence of the total duration of anterograde and retrograde conduction in slow and fast pathways and the AVNRT cycle at the current state of the autonomic nervous system [panels (l) and (o) in Figs. 3, 5, and 7]. However, a few echo beats can arise if the condition for their onset mentioned above is fulfilled [Figs. 4(b) and 5(i)].

As seen in Figs. 2(a), 4(b), and 6(a,b), at the same coefficient γ all kinds of behavior may be observed - a few echo beats, sustained tachycardia, or its termination, depending on the preceding activity. Thus, from the nonlinear dynamics point of view, the sustainability criteria appear to be a basin of attraction [27], when external stimuli at a particular set of initial conditions either lead to persistent oscillations within the AV node ring, which may be accompanied by cycle length variability [28], or to fading echo beats. The nonlinear analysis of the AVNRT behavior is beyond the current work and requires further study.

The shapes of anterograde control conduction curves obtained with S1S2 protocol with different coefficient γ can be with more or less marked tilting and bend at the point of conduction switching between FP and SP [Figs. 3(a), 5(a), and 7(a)]. The bending and the nodal conduction discontinuity became more pronounced with smaller γ. The discontinuity position, hardly observed at large γ, shifted toward a shorter S2 coupling interval due to a significant decrease of aERP_{FP}. The smooth and discontinuous anterograde conduction curves were experimentally demonstrated in rabbits [10, 29] and in humans [24]. The nodal conduction discontinuity appeared in some retrograde control conduction curves with PVC in the second model variant [Fig. 5(b)] was also observed in patients [24, 30] due to the prevalence of rERP_{FP} over rERP_{SP} [Fig. 5(i)].

In most cases of anterograde and retrograde conduction, the vagal modulation affected the ERPs of FP stronger than the ERPs of SP [see panels (f) and (i) in Figs. 3, 5, and 7], as quantitatively demonstrated in [17].

We observed some cases of nodal conduction alternans with the variation of conduction time from beat to beat [31], which are reflected in some bumps on conduction curves in Figs. 3(j), 3(n), 5(j), 5(n), 7(k) and 7(m).

The *spontaneous termination* of AVNRT takes place with increasing refractoriness and nodal conduction delays due to enhanced vagal tone when the sum of anterograde and retrograde conduction delays in SP and FP becomes not equal to the pacing interval, i.e., condition for persistent AVNRT disappears [panels (l) and (o) in Figs. 3, 5, and 7].

In the vast majority of cases, spontaneous termination of AVNRT took place when the conduction was blocked through FP regardless of the AVNRT form [Figs. 2(a), 2(c), 4, 6(a), 6(b), and 8]. The only exception was an echo beat that appeared with PVC during tachycardia in the first model variant [Fig. 2(b)]. This is in line with clinical observations on the spontaneous AVNRT termination [32].

One of the limitations of the current version of the rabbit conduction system model was the absence of heart rate variability. The heart rate variability is also controlled by the balance between parasympathetic and sympathetic ANS tones [33,34]. The second limitation was that we applied the ANS control coefficient γ to SP and FP on the same scale, which led to some differences in their response. In contrast, in reality, the degree of influence of ANS on the AV nodal pathways may differ. Finally, the present structure of the AV node model includes only one slow pathway. Thus, the slow-slow atypical AVNRT form was beyond our consideration.

Conclusions

In this work, we extended the functionality of our previously developed model of the conduction system of the rabbit heart, based on the Aliev-Panfilov cardiac cell model, incorporating control by the autonomic nervous system. The control is accomplished by altering cell refractoriness using a single coefficient, resulting in changes in conduction delays in the AV nodal pathways and intrinsic frequency of pacemaker cells. The effect of the autonomic nervous system spreads from the sinoatrial node to the proximal part of the His bundle simultaneously in all cells of the model.

Using the modified model, we studied conditions for the onset, sustainability, and spontaneous termination of typical and atypical AVNRT forms. The conditions for the onset and sustainability of AVNRT may exist independently in different combinations.

The difference in effective refractory periods between slow and fast pathways and the current state of the autonomic nervous system determines the type of AVNRT at both atrial pacing and His bundle pacing.

The presented updated computationally lightweight but detailed rabbit cardiac conduction model with dual AV nodal pathways is suitable for studying the physiological mechanisms of different forms of AVNRT. Including autonomic nervous system control into the model provides more lifelike functionality and allows the realization of various situations that are nearly impossible to reproduce in animal or human experiments.

References

1. Straus, D. G. & Schocken, D. D. *Marriott's Practical Electrocardiography, 13th ed.*. Philadelphia: Wolters Kluwer Health, 2021.

2. Katritsis, D. G. & Josephson, M. E. Classification of electrophysiological types of atrioventricular nodal re-entrant tachycardia: a reappraisal. *Europace* **15**, 1231–1240 (2013).

3. Nigro, G. *et al.* Autonomic nervous system modulation before the onset of sustained atrioventricular nodal reentry tachycardia. *Ann. Noninvasive Electrocardiol.*, **15(1)**, 49–55 (2010).

4. Appelboam, A. *et al.* Postural modification to the standard Valsalva manoeuvre for emergency treatment of supraventricular tachycardias (REVERT): a randomised controlled trial. *Lancet* **386**, 1747–1753 (2015).

5. Xiao, L., *et al.* Combined modified Valsalva maneuver with adenosine supraventricular tachycardia: A comparative study. *Am. J. Emerg. Med.* **78**, 157–162 (2024).

6. Inada, S., Hancox, J. C., Zhang, H. & Boyett, M. R. One-dimensional mathematical model of the atrioventricular node including atrio-nodal, nodal, and nodal-his cells. *Biophys. J.* **97**, 2117–2127 (2009).

7. Climent, A. M., Guillem, M. S., Zhang, Y., Millet, J. & Mazgalev, T. N. Functional mathematical model of dual pathway AV nodal conduction, *Am. J. Physiol. Heart. Circ. Physiol.* **300**, H1393–H1401 (2011).

8. Plappert, F. *et al.* An atrioventricular node model incorporating autonomic tone. *Front. Physiol.* **13**, 976468 (2022).

9. Ryzhii, M. & Ryzhii, E. A compact multi-functional model of the rabbit atrioventricular node with dual pathways. *Front. Physiol.* **14**, 1126648 (2023).

10. Reid, M. C., Billette, J., Khalife, K. & Tadros, R. Role of compact node and posterior extension in direction-dependent changes in atrioventricular nodal function in rabbit. *J. Cardiovasc. Electrophysiol.* **14**, 1342–1350 (2003).

11. Billette J. & Tadros, R. An integrated overview of AV node physiology. *Pacing Clin. Electrophysiol.* **42(7)**, 805–820 (2019).

12. Ryzhii, M. & Ryzhii, E. Revealing the origin of typical and atypical forms of atrioventricular nodal reentrant tachycardia with a compact computer model of rabbit AV node. *Computing in Cardiology (CinC)*, Atlanta, GA, USA, 2023, pp. 1–4.

13. Aliev, R. R. & Panfilov, A. V. A simple two-variable model of cardiac excitation. *Chaos Solitons Fractals* **7(3)**, 293–301 (1996).

14. Ryzhii, M. & Ryzhii, E. Pacemaking function of two simplified cell models. *PLoS ONE* **17(4)**, e0257935 (2022).

15. George, S. A. *et al.* At the atrioventricular crossroads: Dual pathway electrophysiology in the atrioventricular node and its underlying heterogeneities. *Arrhythmia Electrophys. Rev.* **6(4)**, 179–185 (2017).

16. Hartikainen, J. E., Kautzner, J., Malik, M., Camm, A. J. Sympathetic predominance of cardiac autonomic regulation in patients with left free wall accessory pathway and orthodromic atrioventricular reentrant tachycardia. *Eur. Heart J.* **18(12)**, 1966–1972 (1997).

17. Chiou, Ch.-W,. Chen, Sh.-A., Kung, M.-Ho, Chang, M.-S. & Prystowsky, E. N. Effects of continuous enhanced vagal tone on dual atrioventricular node and accessory pathways. *Circulation* **107**, 2583–2588 (2003).

18. Garfinkel, A. Eight (or more) kinds of alternans *J. Electrocardiol.* **40**, S70–S74 (2007).

19. Šinkovec, M. *et al.* Electrophysiology of anterograde right-atrial and left-atrial inputs to the atrioventricular node in patients with atrioventricular nodal reentrant tachycardia. *Europace* **13**, 869–875 (2011).

20. Morady, F. *et al.* Electrophysiologic effects of epinephrine in humans. *J. Am. Coll. Cardiol.* **11(6)**, 1235–1244 (1988).

21. Cossú, S. F. *et al.* The effects of Isoproterenol on the cardiac conduction system: Site-specific dose dependence. *J. Cardiovasc. Electrophysiol.* **8**, 847–853 (1997).

22. Martin, P. The influence of the parasympathetic nervous system on atrioventricular conduction. *Circ. Res.* **41(5)**, 593–599 (1977).

23. Chen, H. *et al.* Differentiating atrioventricular nodal re-entrant tachycardia from junctional tachycardia: conflicting responses? *Circ. Arrhythm. Electrophysiol.* **8(1)**, 232-235 (2015).

24. Sung, R. J. *et al.* Initiation of two distinct forms of atrioventricular nodal reentrant tachycardia during programmed ventricular stimulation in man. *J. Am. Coll. Cardiol.* **42(3)**, 404–415 (1978).

25. Katritsis, D. G. *et al.* Atypical atrioventricular nodal reentrant tachycardia: prevalence, electrophysiologic characteristics, and tachycardia circuit. *Europace* **17**, 1099–1106 (2015).

26. Katritsis, D. G. *et al.* Coexistent types of atrioventricular nodal re-entrant tachycardia implications for the tachycardia circuit. *Circ. Arrhythm. Electrophysiol.* **8**, 1189–1193 (2015).

27. Izhikevich E. M. *Dynamical systems in neuroscience: The geometry of excitability and bursting.* The MIT Press, 2006.

28. Tamura, S. *et al.* Unique electrophysiological properties of fast–slow atrioventricular nodal reentrant tachycardias characterized by a shortening of retrograde conduction time via a slow pathway manifested during atrial induction. *J. Cardiovasc. Electrophysiol.* **31(6)**, 1420–1429 (2020).

29. Zhang Y. His electrogram alternans (Zhang's phenomenon) and a new model of dual pathway atrioventricular node conduction. *J. Interv. Card. Electrophysiol.* **45**, 19–28 (2016).

30. Wu, D.*et al.* An unusual variety of atrioventricular nodal re-entry due to retrograde dual atrioventricular nodal pathways. *Circulation* **56(1)**, 50–59 (1977).

31. Sun, J., Amellal, F., Glass, L. & Billette, J. Alternans and period-doubling bifurcations in atrioventricular nodal conduction. *J. Theor. Biol.* **173(1)**, 79–91 (1995).

32. Chiale, P. A. *et al.* The mechanisms of spontaneous termination of reentrant supraventricular tachycardias. *Int. J. Cardiol.* **191**, 151–158 (2015).

33. Guzzetti, S. *et al.* Symbolic dynamics of heart rate variability: A probe to investigate cardiac autonomic modulation. *Circulation* **112(4)**, 465–470 (2005).

34. La Rovere, M. T., Porta, A. & Schwartz, P. J. Autonomic control of the heart and its clinical impact. A personal perspective. *Front. Physiol.* **11**, 582 (2020).

Acknowledgements

The work was supported by Japan Society for the Promotion of Science (JSPS KAKENHI) Grant No. 20K12046.

Contributions

Conceptualization: M.R., E.R.; Software: M.R.; Simulations: M.R.; Formal analysis: E.R, M.R.; Methodology: E.R.; Writing the manuscript: M.R, E.R.

Competing Interests Statement

All authors have no conflicts of interest to declare.